We are IntechOpen,
the world's leading publisher of
Open Access books
Built by scientists, for scientists

6,900
Open access books available

186,000
International authors and editors

200M
Downloads

154
Countries delivered to

Our authors are among the

TOP 1%
most cited scientists

12.2%
Contributors from top 500 universities

BOOK CITATION INDEX
CLARIVATE ANALYTICS
INDEXED

WEB OF SCIENCE™

Selection of our books indexed in the Book Citation Index
in Web of Science™ Core Collection (BKCI)

Interested in publishing with us?
Contact book.department@intechopen.com

Numbers displayed above are based on latest data collected.
For more information visit www.intechopen.com

Aluminum Sheet Metal Damage Mechanisms Application to Trimming and Hemming

Helmut Klöcker and Christopher Yukna

Additional information is available at the end of the chapter

Abstract

Aluminum alloys are increasingly used in automotive structural applications thanks to their combination of low density, high strength, and good formability. Appropriate strength levels for dent resistant automotive aluminum panels may be achieved by a combination of alloy design and thermo-mechanical treatments. Unfortunately, increased strength (hardness) generally limits homogeneous plastic deformation. Thus, when shaping complex components large deformation and eventually strain localization, necking and final failure is more likely to occur. In this chapter, we endeavor to explore the best compromises between increased hardening and satisfying formability. Sheet metal shaping generates large strains and eventually strain localization. The accurate measure of metal behavior is discussed first. The following section is dedicated to the kinetics of damage development during shaping. Then metal ductility at low stress triaxiality and consequent strain localization are discussed. Finally, trimming and hemming, the most complex shaping operations to perform efficiently are analyzed providing a powerful tool for alloy design.

Keywords: plane strain compression, extended Bridgman model, damage criterion, trimming, hemming, aluminum automotive alloy design

1. Introduction

Aluminum alloys are increasingly used in automotive structural applications thanks to their combination of low density, high strength, good formability and the bonus of better corrosion resistance. Appropriate hardness levels for dent resistant automotive aluminum panels (doors, hoods) may be achieved by a combination of alloy design and thermo-mechanical treatment. To insure adequate hardness values, most aluminum automotive alloys contain large amounts of hard intermetallic particles. In ductile metals, voids are first nucleated by decohesion or cracking of these second phase particles and then grow until they eventually coalescence to

form a macroscopic crack. Hence, increased strength (hardness) generally limits homogeneous plastic deformation. In the early 70s a new branch of material science ("the local approach of ductile fracture"), was initiated by the pioneering contributions of Gurland and Plateau [1], McClintock [2], Rice and Tracey [3], Koplik and Needleman [4], Gurson [5], Le Roy et al. [6], Hutchinson and Tvergaard [7]. One outcome of all these publications is the major role played by stress triaxiality. Furthermore, Marciniak and Kuczynski [8] highlighted the tremendous effect of strain localization when sheet metal is submitted to large strains. Unfortunately, shaping complex components imposes large deformations and eventually strain localization.

In Section 2, we outline the accurate characterization of the sheet material behavior at large strains by adequate compression tests. Next, the measurement of the macroscopic strain to failure by standard tensile tests is offered. In the same section, the relation between this macroscopically determined characteristic and the local strain and stress triaxiality field is analyzed. Then, the kinetics of strain localization causing damage is presented. As aforementioned, we end with two particularly discriminating forming operations, trimming and hemming, which are examined in detail.

2. Characterization of sheet metal behavior

During deep drawing or cutting operations of sheet metal local strains up to 200% are reached. Hence, large deformation compression and tensile tests on rolled sheets reveal the necessity for finite element simulations of machining and forming operations. In Section 2.1, the most commonly used compression tests providing sheet metal characterization are shown. These determine material behavior under large strains without significant damage. As sheet shaping and forming operations are limited by necking and consequent failure, Section 2.2 will demonstrate how to determine the failure strain by classic tensile tests.

2.1. Measuring stress-strain curves to large strains on sheet metal

Due to necking, only comparatively small strains can be attained in standard tensile tests. Standard uniaxial compression tests on cold rolled sheets (typically 1 mm thickness) are also impossible due to friction. Finally, torsion tests on cold rolled 1-mm-thick sheets would lead to extremely small sample sections. In this section the experimental techniques particularly suited for high strain characterization will be presented.

Half a century ago, Watts and Ford [9] introduced the **P**lane **S**train **C**ompression punching technique to determine the room temperature behavior of strip metal by compressing by means of a punching tool which is longer than the test-piece. However using this technique, the sheets can only be compressed along the normal axis. The maximum strain is much less than unity and the deformed sample volume is very small. Recently, Vegter et al. [10] determined the initial yield stress of sheet metal by several tests (tension, plane strain tension, compression of layered samples and shear tests). The tension and compression tests are limited to strains smaller than 0.2 and the shear test is restricted to strains smaller than 0.4.

The *channel-die test* is an alternative plane strain compression test without any lateral spreading, but which was then relatively unknown and has so far been relatively little employed. Maurice and Driver [11, 12] have developed original hot channel-die equipment which has the advantage of imposing true plane strain compression without major friction as shown by Bacha et al. [13]. **Figure 1** shows a schematic of the channel-die apparatus first described by Maurice and Driver [11]. The channel is composed of 3 separate steel plates of which the center plate has the same thickness (7 mm) as the punch width. The equipment of **Figure 1** was installed in an a Schenck 100 kN servo-hydraulic machine whose electronic and hydraulic control systems enable constant plastic strain rate tests up to about $20\ \mathrm{s}^{-1}$ (according to sample dimensions). Loads are measured by standard load cells and displacements by means of a linear variable differential transformer (LVDT transducer) situated between the crosshead and the base of the channel-die. More details concerning the channel-die equipment can be found in the original papers [11, 12]. Channel-die tests have also been used for room temperature testing on mono-block samples [14].

To our knowledge, Bacha et al. [15] were the first to apply PSC to layered sheet specimens (**Figure 2**). The sheets were machined to obtain seven strips 1 mm thick 9.01 mm high and 10.01 mm long and bonded with standard cyanoacrylate glue. The sample preparation is crucial to insure plane mutually orthogonal surfaces. The specifics can be found in Bacha et al. [15]. The area reduction due to the glue layer is thus smaller than 1%. Since four major surfaces of the sample are in contact with the tools, it is wrapped in a PTFE (Teflon) ribbon (50 μm thickness).
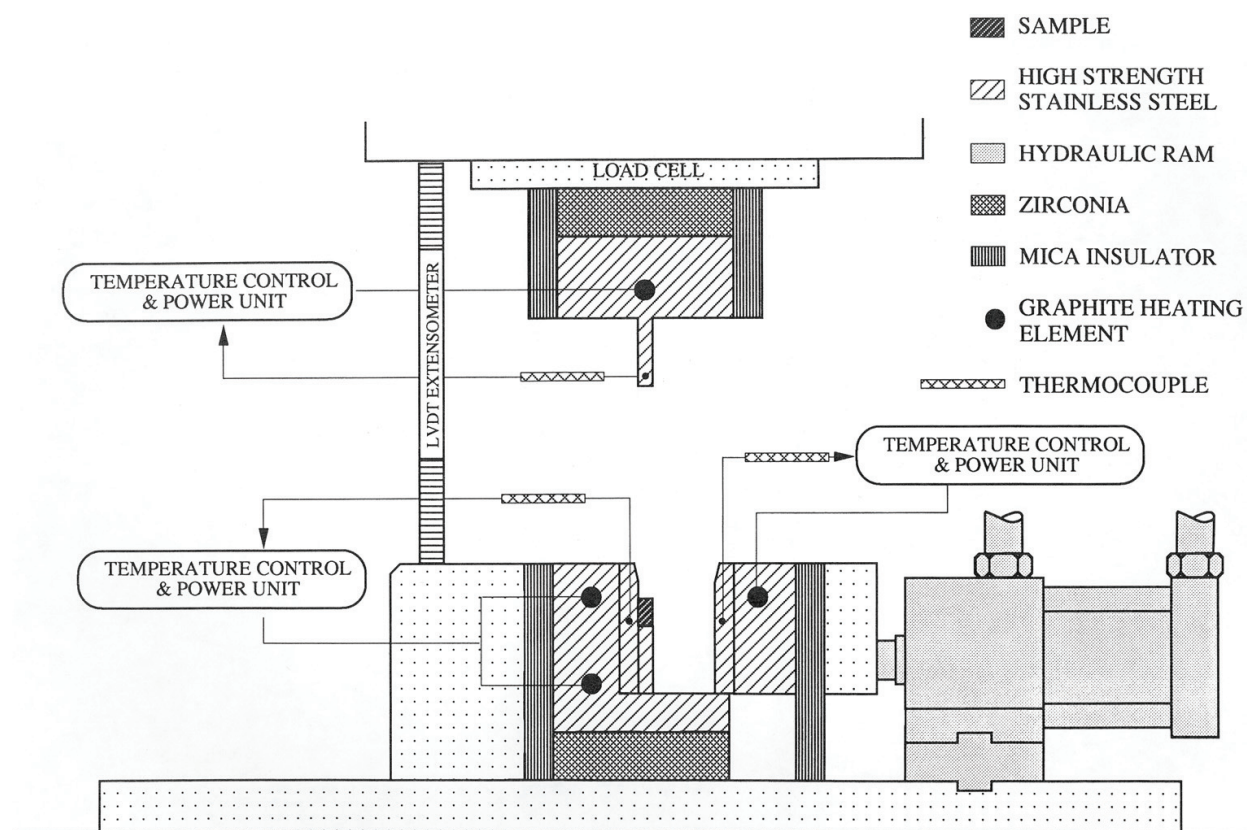

Figure 1. Schematic of the channel-die equipment [11].

Bacha et al. [15] compressed two aluminum alloys, AA5182 and AA6016, widely used in sheet forming particularly in the automotive industry, at a constant strain rate of 10^{-1} s^{-1}, by channel-die compression. For the AA6016 alloy two different grades (*a, b*) were considered. **Table 1** gives the chemical composition of the alloys.

Brunet and Morestin [16] determined the Langford coefficient of the AA6016 sheets by tensile tests and showed that the anisotropy is negligible for the two grades of AA6016. The 5182 alloy was compressed along rolling and transverse directions and revealed in plane isotropy.

To determine reliable stress-strain curves, particular attention should be paid to the influence of the PTFE-layer and the compliance of the test rig. The displacement was corrected to take into account the deformation of the test rig and the PTFE-layer [17]:

$$d_{corrected} = \left(d_{measured} - \frac{Q_{measured}}{k}\right)\left(1 - \frac{h_{PTFE}}{h_0}\right) \tag{1}$$

h_0 and h_{PTFE} designate the initial sample and PTFE-layer thicknesses. $d_{measured}$ is the displacement measured by the LVDT and $d_{corrected}$ takes into account the deformation of the PTFE layer. $Q_{measured}$ is the measured load. k is the stiffness of the test rig and was determined by measuring the punch displacement without a sample present in the channel (k = 91 kN/mm). The measured load has been corrected to take into account friction effects [17] as follows:

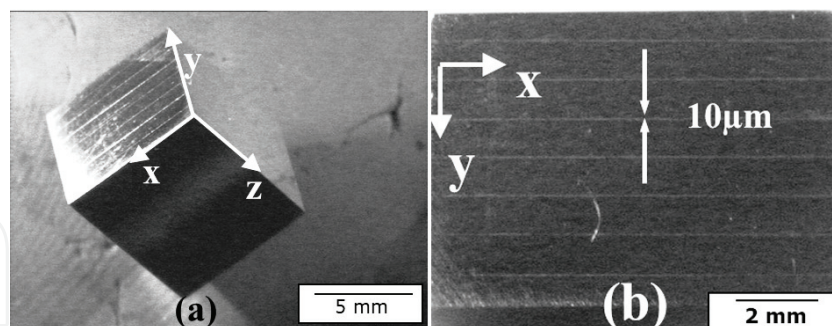$$Q_{corrected} = \frac{Q_{measured}}{1 + \frac{\dot{W}_F}{\dot{W}_P}} \tag{2}$$

Figure 2. Layered sheet sample (a) 3D view, (b) view along the direction of the compression z.

Grade	Mg	Si	Cu	Fe	Mn
5182	4.25	0.09	0.06	0.29	0.35
6016 (a)	0.33	1.03	0.12	0.3	0.11
6016 (b)	0.43	0.98	0.15	0.3	0.11

Table 1. Chemical composition of the different grades.

where $Q_{corrected}$ is the corrected value of the applied load $Q_{measured}$. $\dot{W}_F$ and $\dot{W}_P$ are the work rates associated respectively to friction and to plastic deformation. The ratio between these work rates was estimated by [17] as

$$\frac{\dot{W}_F}{\dot{W}_P} = \frac{\overline{m}}{12\,l_0\,h_0\,e_0}\left[\frac{l^3}{4}\ln\left(\frac{Z+2h}{Z-2h}\right) + 2\,h^3\ln\left(\frac{Z+l}{Z-l}\right) + 2\,lhZ + l^2e_0\right] \tag{3a}$$

$$Z = \sqrt{l^2 + 4h^2} \tag{3b}$$

where $\overline{m}$ is the Tresca friction coefficient. h_0, l_0, and h, l are respectively the initial and current sample height and length. e_0 corresponds to the sample and channel width (7 mm).

To determine the equivalent stress $\overline{\sigma}$ and the equivalent strain $\overline{\varepsilon}$, the overall load was corrected by Eqs. (2), (3a) and (3b) with a value of $\overline{m} = 0.02$. However the shear stresses and strains due to friction were neglected, i.e., the stress and the strain rate tensors were assumed diagonal. Thus, the equivalent von Mises stress and strain may be written:

$$\overline{\sigma} = \frac{\sqrt{3}}{2}\sqrt{\frac{Q_{corrected}}{e_0l_0}\left(1 - \frac{d_{corrected}}{h_0}\right)}, \quad \overline{\varepsilon} = \frac{2}{\sqrt{3}}\ln\left(\frac{h_0}{h_0 - d_{corrected}}\right) \tag{4}$$

Figure 2 shows equivalent stress *vs.* equivalent strain curves for all the grades. To represent the material flow stress, σ_Y, at large deformations an extended Voce model [18, 19] has been chosen.

$$\begin{cases} \sigma_Y = \sigma_{Y_0} + (\sigma_\infty - \sigma_{Y_0})\left(1 - \exp\left(-\delta\overline{\varepsilon}_p\right)\right) + \alpha\overline{\varepsilon}_p \\ \overline{\varepsilon}_p = \overline{\varepsilon} - \dfrac{\sigma_Y}{E} \end{cases} \tag{5}$$

E is the Young's modulus. $\overline{\varepsilon}$ and $\overline{\varepsilon}_p$ are respectively the total and the plastic equivalent strain. σ_{Y_0} is the initial flow stress. σ_∞ corresponds to the stress at very large plastic strains in the Voce model. $\alpha\overline{\varepsilon}_p$ is an additional term accounting for small positive strain hardening at very large plastic deformation. The initial flow stress σ_{Y_0} was determined previously in simple tension. **Table 2** summarizes the coefficients of the different Voce models. The most significant results are the different values of the α parameter for 5182 and 6016 alloys (**Figure 3**).

To assess the validity of the experimental method described above, Bacha et al. used the flow rule (5) and reproduced the experimental load displacement curves by finite element model [15]. Moreover, the finite element calculations showed that, using a Teflon film, the friction

Grade	E (GPa)	σ_o (MPa)	σ_∞ (MPa)	δ	α (MPa)
AA5182	70	130	264	14.6	101
AA6016a	70	130	310	16	15
AA6016b	70	100	248	12	14

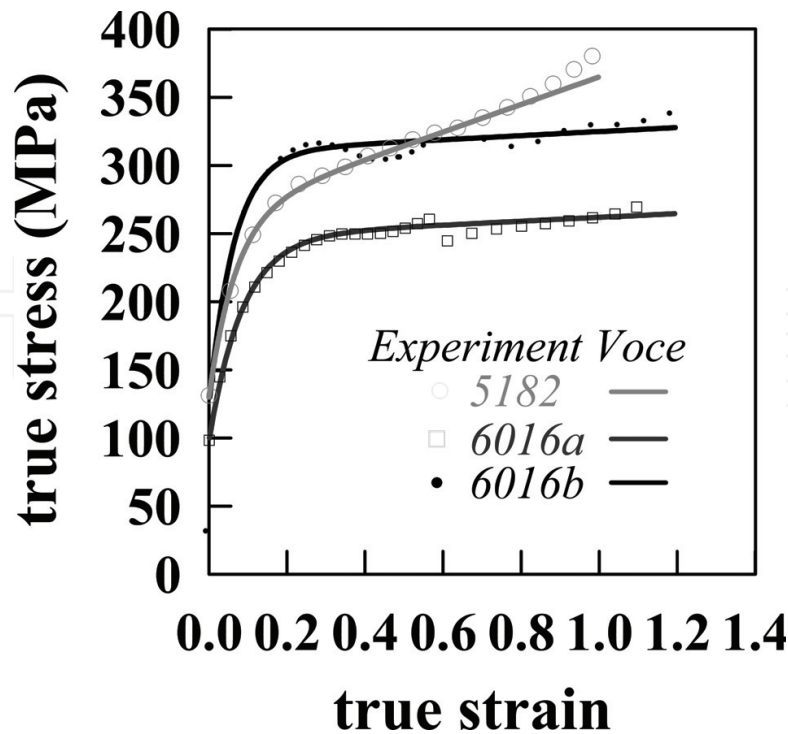**Table 2.** Voce model parameters for the AA5182 and AA6016 grades.

Figure 3. Measured true stress-strain curves compared to extended Voce model.

coefficient between the test sample and the tool is less than 0.02 and the friction coefficient between different layers of the sample only play a very minor role. The sample deforms homogeneously over more than 80% of its volume irrespective of interlaminate (glue) behavior.

Barlat et al. [20] measured the initial yield surface by biaxial compression tests on cubic specimens made from laminated binary Al-Mg alloy sheet samples. They used an expensive biaxial compression testing machine. Because of the physical constraints of the loading dies, their deformation step was limited to a strain of about 0.1. This technique was more costly than the simple one presented here.

To our knowledge all previous methods (tension, shear, and compression) measure the initial yield strength but are not very useful for analyzing the strain hardening of the material. The PSC method is therefore complementary to these techniques, and hence particularly useful for obtaining large-strain material behavior. However, very thin sheets (of thickness less than 1 mm) are also widely used in industry. The stress-strain curves of these sheets are even more difficult to obtain than the stress-strain curves of the larger 1 mm ones. Determining the minimum layer thickness that avoids instabilities and gives reliable results in plane strain compression would be interesting for ultra-thin sheets.

For ductile materials, damage consists of void nucleation around intermetallic particles. These cavities grow and coalesce up to the development of a crack and sample failure. Historically, hole growth and coalescence have been analyzed by unit cell calculations consisting of finite element simulations on a representative material element containing a single void [4, 21, 22]. During deep drawing or cutting operations local tensile and shearing strains up to 200% are

reached. As a consequence, to satisfactorily simulate and thoroughly analyze shaping operations, the following material description is needed:

1. The $\sigma(\varepsilon)$ curves for large deformations up to 200%;

2. The local strain at failure in tension;

3. A definition of a damage variable and the determination of its critical value for complex stress-strain paths accurately corresponding to shaping operations.

The present section outlined some experimental procedures for determining large-strain $\sigma(\varepsilon)$ curves. The following will offer an approach for measuring the strain to failure by simple tensile test on sheet material specimens [23–25].

2.2. The strain to failure in sheet metal

Historically, ductility is defined by the area reduction at failure ($\ln(A_r/A_0)$) in a tensile test. A_r and A_0 designate respectively the initial and final cross-sectional area. Siebel and Pomp [23] and Bridgman [26] developed expressions for the true stress-strain curves in the neck of axisymmetric tensile specimens. Subsequently Needleman [27] and Le Roy et al. [6] studied the necking of axisymmetric specimens by finite element analysis. In uniaxial tensile tests on ductile rate-independent sheet material, plastic instability and flow localization occurs just after the maximum load when diffuse necking starts. But, after the onset of a diffuse neck, deformation continues under a falling load until the development of a localized neck then ductile fracture [28]. Secondary strain localization depends on the shape factor (width/thickness) of the tensile test-piece and the material strain hardening [29]. Large width/thickness ratios and small strain hardening parameters lead to localization in the width of the specimen. Whereas, small width/thickness ratios and large-strain hardening parameters cause through-thickness localization.

As mentioned previously, most aluminum automotive alloys contain large amounts of intermetallic phases. **Figure 4** shows typical micrographs of the two AA6016 grades [30]. These contain Fe_mAl_n or Mg_2Si particles. Void nucleation and growth around intermetallic particles may occur [31] and eventually failure happen.

Ductile failure is largely controlled by stress triaxiality at the core of the sheet even though this is often considered in two dimensions. The stress triaxiality T corresponds to the ratio between the mean stress σ_m and the equivalent von Mises stress $\overline{\sigma}$

$$T = \frac{\sigma_m}{\overline{\sigma}} \tag{6}$$

Void growth during overall straining was shown to increase exponentially with the stress triaxiality. Early models describe the growth of a single cavity in an infinite elastic plastic solid [2, 3] or an infinite viscoplastic solid [32, 33]. Finite void volume fractions were addressed first by the plane strain analysis of Needleman [27] representing a square array of cylindrical voids. Gurson [5] determined an analytical expression for the stress potential of a spherical volume of elastoplastic material containing a concentric spherical void. Tvergaard [34] used an
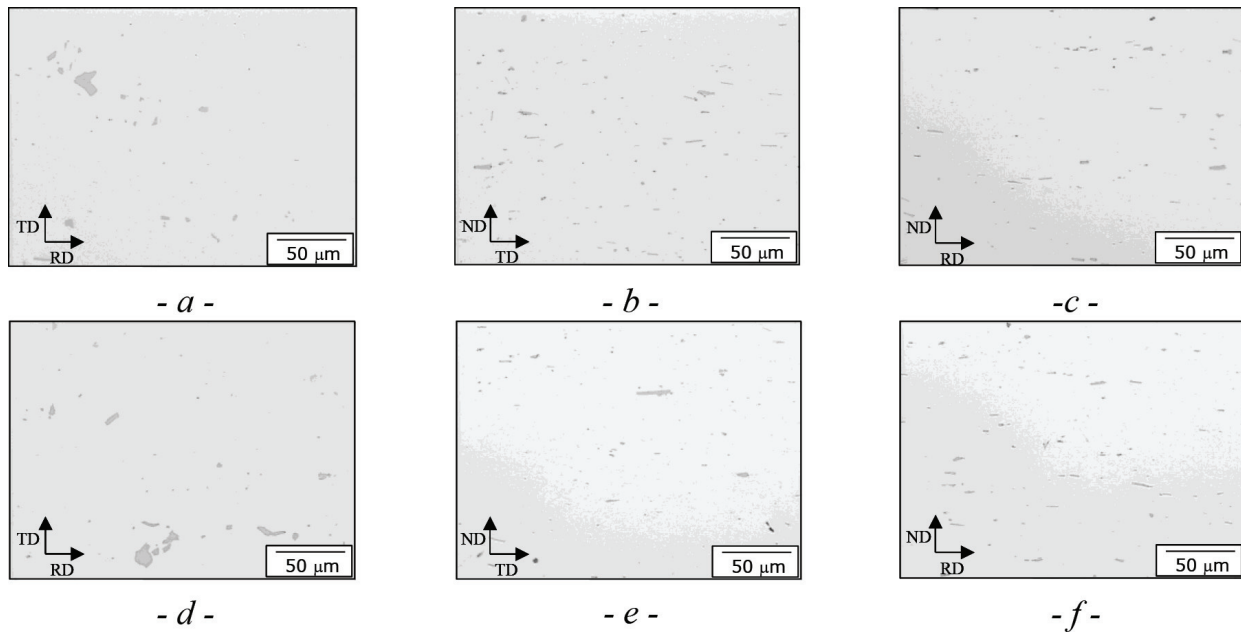
Figure 4. FEG-SEM pictures showing the typical microstructure of the two AA6016 grades: *a* (a,b,c) and *b* (d,e,f).

axisymmetric cell model to represent a periodic array of spherical holes. All these models can be summarized by expressing the void volume growth as follows [35]:

$$\frac{V(\varepsilon_p)}{V_0} = A \exp\left(\alpha \exp\left(T - 1/3\right)\varepsilon_p\right) \tag{7}$$

ε_p is the equivalent plastic strain of the material surrounding the void, V_0 the initial and V the current void volume. A is constant depending on the model chosen. The coefficient α may take rather complex expressions in the different models. Nevertheless, the cavities grow exponentially with the plastic strain when stress triaxiality T is larger than 1/3. The fundamental role of the stress triaxiality parameter will be discussed hereafter.

Bacha et al. [36] ran tensile tests on the previously mentioned AA6016 alloys. **Figure 5** shows the initial sample geometry and the shape at failure. Tensile tests on sheet metal (rectangular cross-section) obviously cause heterogeneous deformation in the cross-section. Due to strain localization in the minimum section of test samples with a rectangular cross-section, the macroscopic measurement does not provide satisfactory results. This section presents a simple method for measuring true strain to failure by simple tensile tests on sheet metal.

The method to determine the macroscopic strain at failure is outlined in Bacha et al. [36]. The macroscopic strains to failure for both alloys were found equal to 0.67 for grade *a* & 0.87 for grade *b* respectively. In the same work, the local strain field was determined by FE simulation based on the material behavior characterized by PSC. **Figure 6** shows the FE-predicted geometry of grade *a* sample at failure and equivalent plastic strain (ε_p) in the minimum cross-section. The center of the specimen exhibits a maximum plastic strain of 0.91, much higher than the macroscopic value. The second illustration in **Figure 5** corresponds to the stress triaxiality distribution.
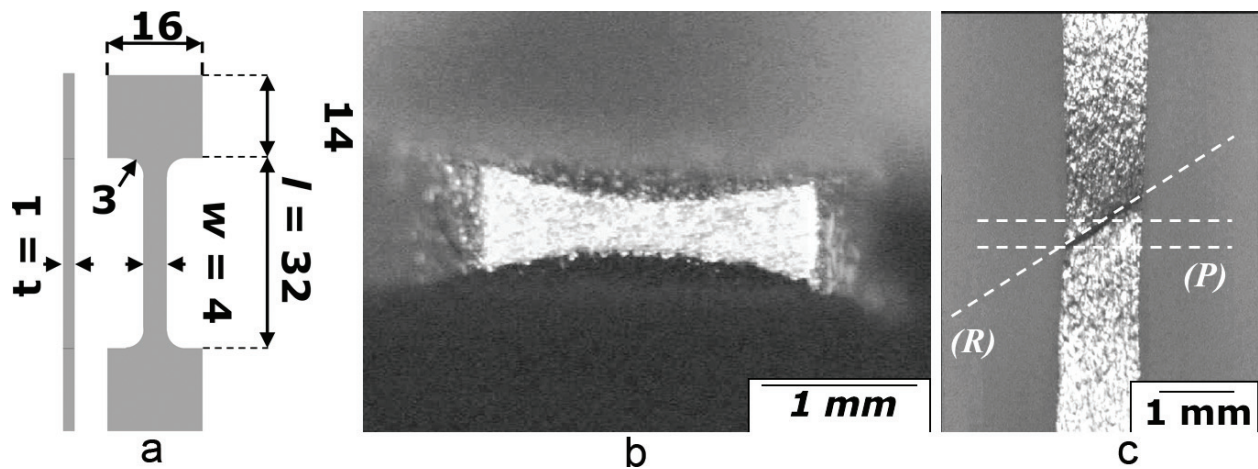
Figure 5. Tension specimen (width w = 1 mm), the thickness (t = 1 mm) corresponds to the thickness of the rolled sheet and height (l = 32 mm). (a) Initial shape, (b) optical view of cross-section after failure and (c) specimen close to failure.
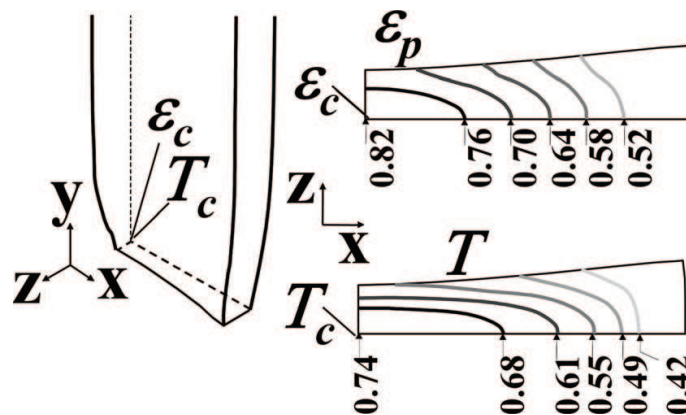

Figure 6. AA6016 grade *a*. Finite element simulation results: overall specimen shape at failure. Equivalent strain and stress triaxiality maps in the minimum section.

Seeing the primary importance of this parameter on damage severity, the variation in the cross-section highlights the damage development in the center of the specimen.

As ductile void growth rate increases exponentially with stress triaxiality, small errors in the estimation of triaxiality lead to large differences in the cavity growth rate and poorly predict material ductility. Even for materials with constant strain hardening, Bridgeman's analysis of the stress triaxiality in axisymmetric tensile specimens may not be extended to tensile specimens with rectangular cross-sections.

According to the present analysis, the strain and stress gradient in rectangular cross-section tensile specimens of is clearly larger than in axisymmetric samples. For material ductility analysis, the local stress-strain in the central area has to be known precisely. The classic Bridgman model was developed for axisymmetric specimens and therefore underestimates the stress triaxiality at the center.

The center stress and strain depend on the pre and post-necking material behavior. The influence of hardening and the post-necking strain on test-piece center stress and strain may be analyzed separately only for constant strain hardening. Only for these academic material laws, the area reduction may be used to predict the center stress and strain. For actual materials with variable strain hardening, the influence of the post-necking strain and material behavior on the stress and strain field in the specimen center may not be separated. Hence, the macroscopic strain given by the area reduction in the minimum section may not be used to characterize the strain and stress in the center of the piece, nor to define material ductility. The extrapolation of $\sigma(\varepsilon)$ determined by tensile tests to large-strain behavior predicts erroneously ductility. To determine correctly the true ductility of the material in question, the $\sigma(\varepsilon)$ curves have to be measured previously by compression tests (Section 2.1) and the tensile test has to be analyzed by FE-calculations.

Obviously, the values predicted for the strain at coalescence and the experimental values of the failure strain are very close. Including damage during the tensile test prior to cavity coalescence by a Gurson-like model is possible in principle. But damage prior to void coalescence only slightly affects the projected values of strain at coalescence. In addition, the parameters required as input for a modified Gurson model are not yet well established. Moreover, in present alloys, secondary void nucleation and growth around smaller particles may be observed and have more influence. Precisely taking into account this secondary cavity coalescence requires a robust model for void nucleation. With a minimum of reasonable and verified assumptions, the local strain in the specimen center at failure should be predicted very accurately. Sheet metal large-strain behavior was obtained by PSC (Section 2.1), and the strain to failure by a simple tensile test (Section 2.2). Most shaping or forming operations correspond to straining under small stress triaxiality. The ductility (strain to failure) under such loading conditions will be analyzed next.

3. Damage development in sheet metal trimming and hemming

3.1. Metal ductility at low stress triaxiality

Large stress triaxiality values (T > 0.4) decrease the fracture strain (ductility). Thus, during the last 20 years, most research efforts dealt essentially with medium to high stress triaxiality loadings. But, in many forming operations, the material is submitted to large compressive or small tensile loads corresponding to negative or small stress triaxiality loadings. In this context, Bao and Wierzbicki [37] deformed an AA2024 alloy under various stress-strain paths covering small and large values of the stress triaxiality; their results are summarized on **Figure 7** [30]. The high stress triaxiality results are well described by the damage models outlined in Section 2. However, when stress triaxiality is small, these approaches significantly over-estimate the strain to failure and hence cannot forecast forming limit diagrams.

Bacha et al. [30, 38, 40] analyzed shearing of the two AA6016 sheets characterized previously in PSC. During trimming or hemming of heterogeneous materials, the second phase particles undergo large displacements. **Figure 8a** and **b** illustrate the microstructural changes observed
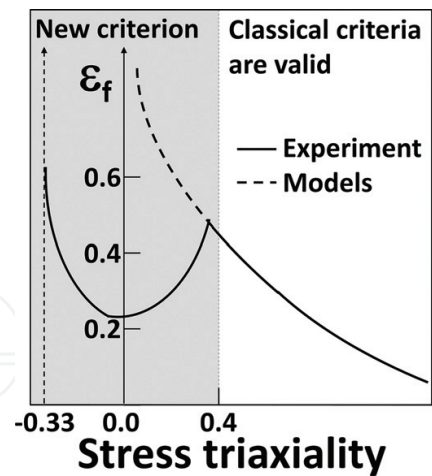
Figure 7. Strain to failure as a function of the stress triaxiality as measured by Bao and Wierzbicki [37] and predicted by Bacha et al. [30].
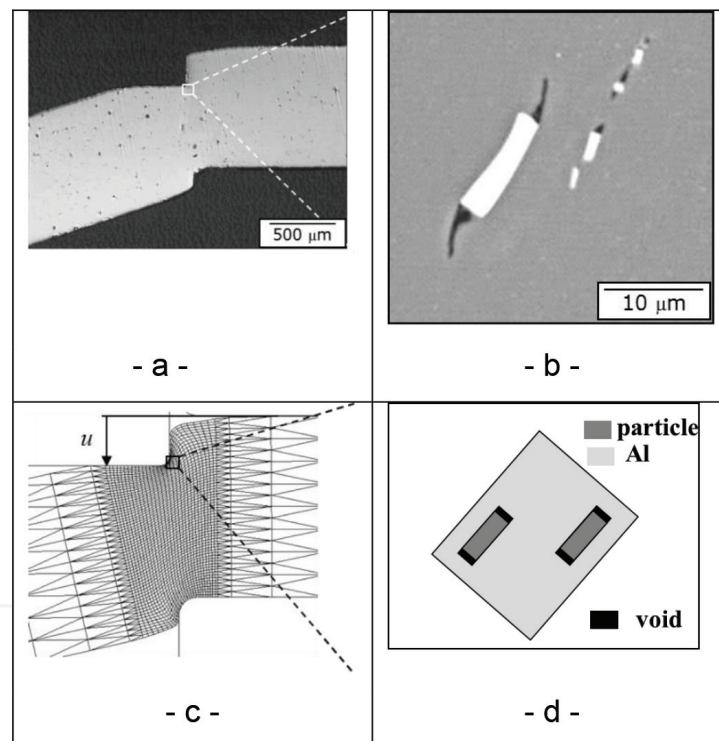

Figure 8. Shearing of an AA6016 grade **a** sheet. (a) Overall shape, (b) intermetallic particle orientation, (c) simulated overall shape, and (d) simulated intermetallic particle orientation.

and subsequently simulated during cropping of a AA6016 grade *a* sheet. The intermetallic particles (Mg$_2$Si) are initially aligned in the rolling or transverse directions (**Figure 4**). The shearing (**Figure 8a**) generates significant rotations and smaller particle distances (**Figure 8b**). Nevertheless, the broken particle matrix interface lost its load carrying capacity. Hence, subsequent failure occurs due to the reduction of inter-particle spacing and subsequent strain localization. Based on Thomason's void coalescence model [41], Bacha and co-workers [30] developed a method to describe strain localization due to reduced inter-particle spacing after

large material rotations. **Figure 8** highlights the comparison between experimental and FE-predicted particle orientation. The corresponding damage criterion, valid at small stress triaxiality and large material rotations, is applied to trimming in the third section.

3.2. Trimming of aluminum automotive sheets

After stamping, the final shape of car body panels is achieved by cutting or trimming. Metal cutting is a complex three-dimensional process [42]. However, the physics of this process can be understood by a 2D model. Early work on blanking used macroscopic analysis. Deformation localizes in a small band below the blade. Its width is controlled by the material. At the beginning of the cutting process, the stress in the sheet corresponds to simple shear. During the cutting process, tension stress increases [43, 44]. However, to properly analyze the stress-strain concentrations close to the blades observed in the actual process, a finite element model is essential. The three principal parts of a trimming machine are the blade, sheet and die (**Figure 9**). Other elements may also be added like a blank holder, and sometimes a scrap holder to prevent sheet bending. The following parameters describe the geometry of the plane cutting process:

• Sheet thickness T,

• Cutting angle α, i.e., the angle between the sheet normal and the direction of blade displacement

• Clearance C between the blade and the die, i.e., the distance between the cutting section and the die

• Blade (R_{blade}) and die radii (R_{die}),

• Blade displacement U

Cutting a sheet generates a work piece and scrap. Here, the work piece is maintained under the blank holder after cutting. Trimming or cutting an infinitely ductile material with no clearance, would generate a straight cutting path. Actually, the presence of the clearance and finite material ductility produce more complex cutting paths with various characteristic zones (**Figure 10**):
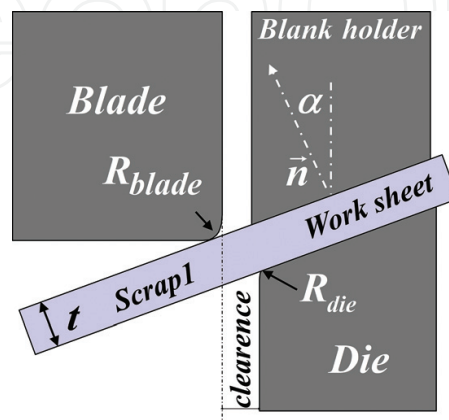

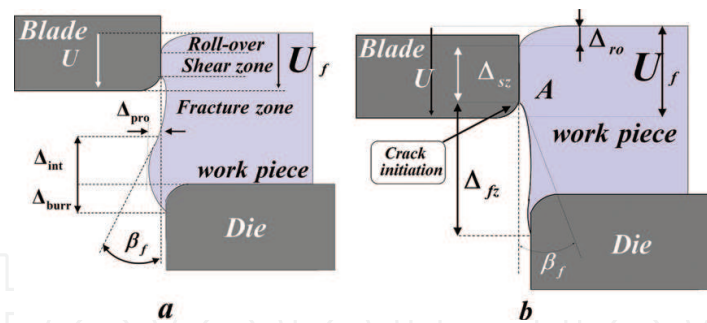**Figure 9.** Schematic of the planar sheet trimming process.

Figure 10. Schematic representation of plane trimming process. Cut generating slivers (a), cut profile without slivers (b) [40].

- Roll-over (height Δ_{ro}) corresponds to elastoplastic shearing of the sheet material,

- Sheared zone (height Δ_{sz}) corresponds to indentation of the sheet material,

- Fractured zone (height Δ_{fz}),

- Burr (height Δ_{burr}) depending on the crack path at the final stage of the process.

Two other crucial geometrical parameters associated with the cutting path are:

- Blade displacement at crack initiation U_f,

- Angle between the fractured zone and the blade displacement direction β_f

During the trimming process, small filaments of hardened material called slivers may be produced (**Figure 10b**). Li and co-workers observed sliver generation when cutting AA6111T4 and AA6022T4 alloys [45–47]. **Figure 11** shows slivers observed when shearing the AA6016 (grade *a*) sheet [38].

Bacha et al. [38–40] characterized the trimming of two steel alloys (1 and 2), plus a 5000 series and three 6000 series aluminum alloys. In order to analyze the influence of the material behavior on the crack path, the tool geometry was aligned to a reference configuration. The values of the parameters of the following industrial tool set-up are frequently documented. The clearance C, the blade (R_{blade}) and die (R_{die}) radii were respectively 5, 5 and 10% of the sheet thickness T. ({c, R_{blade}, R_{die}} = {0.05, 0.05, 0.10}). The cutting angle α was zero, and no scrap holder was used. **Figure 12** shows the corresponding fracture surfaces. The results prove that sliver generation is related to small values of the sheared zone Δ_{sz}.

Cutting AA6016 (grade *a* and *c*) alloys, in the reference tool configuration, induces slivers. Thus, the parameters controlling the tool geometry were changed. The results show that enlarging the blade radius (R_{blade} = 0.3) as well as an increase of the cutting angle (α = 20°) or the use of a scrap holder completely prevent convex cracking (**Figure 13**). Increasing the clearance does decrease the blade-bulge interaction but does not completely prevent slivers.

The clearance and the scrap holder influence the specimen sheet geometry. All other parameters influence directly the height of the sheared zone Δ_{sz}. The height of the sheared zone Δsz depends on the blade displacement at crack initiation U_f:
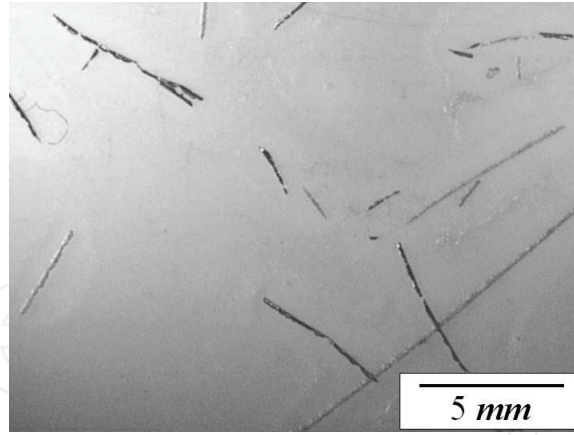
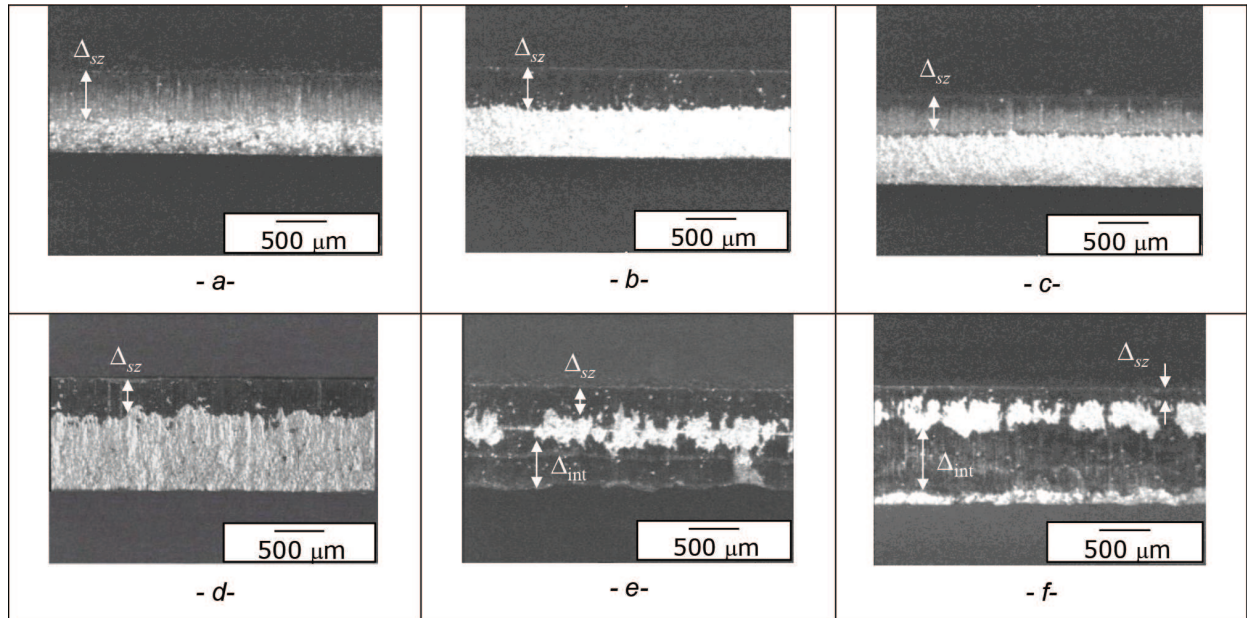**Figure 11.** Example of slivers generated on a AA6016 (grade a) sheet.

Figure 12. Fracture surfaces of trimmed alloys. The shear zone height decreases from a to f: (a) steel 1, (b) AA5182, (c) steel 2, (d) AA6016 (grade **b**), (e) AA6016 (grade **c**), (f) AA6016 (grade **a**).

$$u_f = \frac{U_f}{t} = \frac{\Delta_{sz} + \Delta_{ro} + R_{blade}}{t} \qquad (8)$$

The experimental results reveal that small values of the blade displacement at crack initiation ($u_f < 0.3$) lead to convex cracking and slivers proliferation. Conversely, if u_f is larger than the threshold 0.3, no convex cracking is observed. Bacha et al. [38–40] confirmed this by the finite element model outlined in Section 3.1.

During trimming, the material undergoes locally severe rotations leading to a rearrangement of the intermetallic particles and consequent strain localization. This localization controls the blade displacement at crack initiation and hence both the crack path and sliver production.
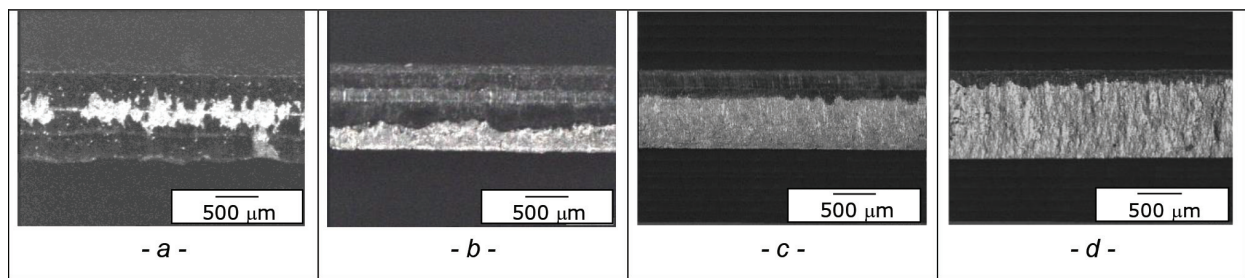
Figure 13. Influence of the tool geometry on the fracture surface of AA6xxx-**b**: (a) reference geometry, (b) increase of the blade radius, (c) increase of the cutting angle, (d) use of a scrap holder.

In the next section, we address hemming, another process essential to sheet forming that leads to significant strain localization.

3.3. Hemming of aluminum automotive sheets

Bending is important in the shaping of complex parts and also critical in the attachment of outer skins to inner sheet panels by hemming. Appropriate strength levels for automotive aluminum panels are achieved by a combination of alloy conception and thermo-mechanical treatments [48, 49]. Several experimental studies underlined the influence of alloy composition on bend performance of Al 6xxx automotive sheet [50, 51]. The bendability has been shown to decrease with increasing copper, iron and Si content.

Most theories attribute bending damage to the development of surface roughness and intense strain localization. Several authors conclude that shear bands initiate at points of strain concentration induced by initial thickness heterogeneity [7, 52, 53]. Other authors have analyzed the effects of thermal softening on shear banding. Crystal plasticity simulations have also been used, essentially to analyze the effect of particular textures on the formability and bendability of sheet metal [28, 52, 54–56]. Probably the chief consensus of these studies is the close relationship between surface roughening and strain localization. But strain localization is difficult to characterize experimentally. Therefore, most experimental studies have compared different alloys based on macroscopic measurements (bend angle), whereas theoretical damage analyses focus on local behavior (shear band pattern).

Several tests to characterize bend performance have been described in the literature [57, 58]. Mattei and co-workers [59, 60] characterized bendability of 6016T4 sheet metal by the standardized Daimler-Chrysler (DIN 50 111). The test set-up is shown in **Figure 14**. During the bend test the applied force F and the punch displacement U were recorded continuously.

Figure 15a shows a typical load displacement curve for the 6016T4 sheet with a punch displacement at failure U_f of 12.8 mm and a minimum bending angle β_f of 28°. The apparent rigidity (dF/dU) plotted in **Figure 15b** exhibits a clear maximum at 0.92 U_f. A crack develops "suddenly" at a punch displacement of 0.92 U_f corresponding to the maximum of the overall rigidity [60]. Crack formation during a standard bend test occurs when the overall rigidity attains a maximum.

Mattei et al. [60] compared the bendability of samples with an industrial surface finish and mirror polished samples. Initial surface roughness (undulations) favors the strain localization. But eliminating the surface roughness at an intermediate bending angle does not enhance the bendability compared to an initial mirror surface finish. **Figure 16** shows an optical
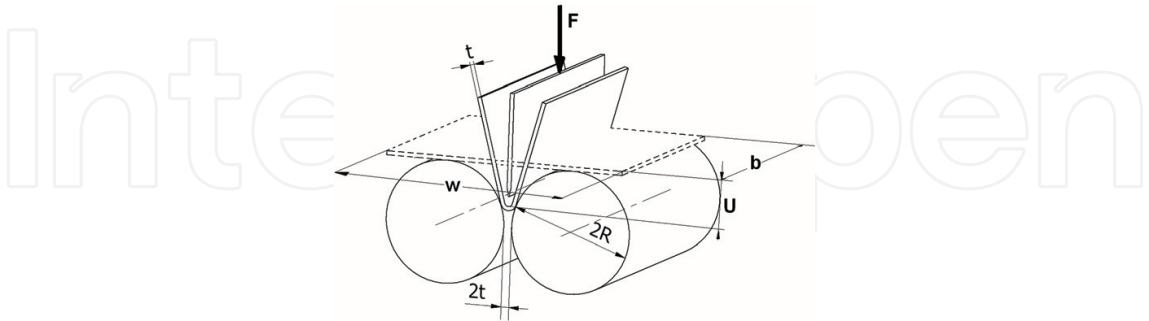

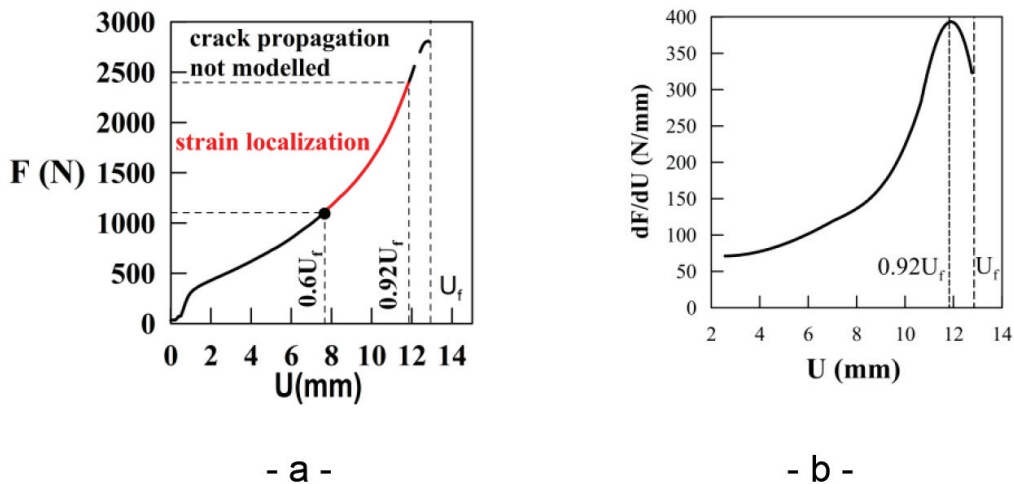**Figure 14.** Bending test overall view according to DIN 50 111.

- a -   - b -

Figure 15. Standard bending test on AA6016 1 mm sheet. (a) Typical load displacement and (b) rigidity displacement curve.
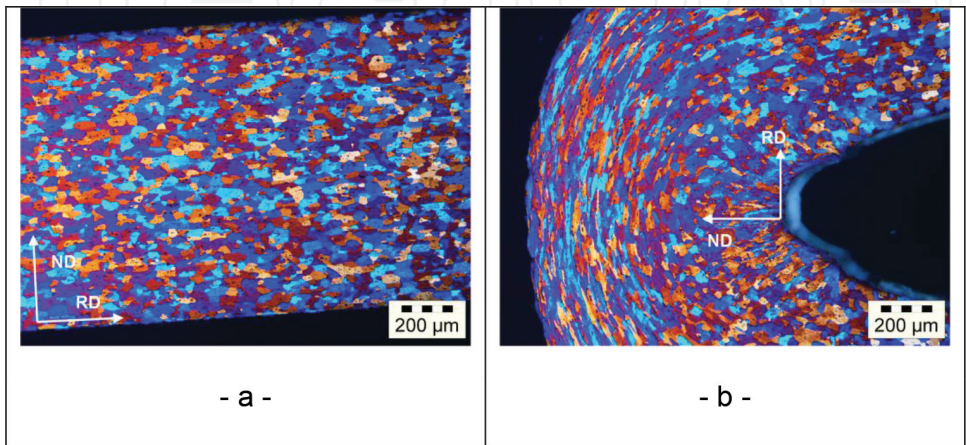

- a -   - b -

Figure 16. Optical micrograph of the initial microstructure (a) and after bending to failure (b).

micrograph of a sample bent to the minimum bend angle. Strain localization leads to significant changes in grain shape and orientation. Grain rotation and deformation at the outer surface lead to surface undulations. This experimental work clearly shows that through-thickness strain localization controls damage development during AA6016 sheet bending.

Mattei et al. [61] developed a finite element microstructure based model of the standard bending test to predict strain localization. The sheet metal is modeled as a grain aggregate, each grain with its own flow stress. This simple model facilitates industrial AA6xxx sheet alloys conception by correctly describing the respective influences of sheet thickness, grain size and shape, and work hardening. In particular, this model brings out the primary importance of large-strain hardening and the flow stress spatial distribution. It can be used to furnish simple guidelines for designing highly bendable sheet metal.

4. Conclusion

First, we showed PSC, a relatively easy and reliable method for determining large-strain (σ,ε) curves on sheet metal. In other words, layered sheet metal samples can be deformed in channel-die (plane strain) compression up to strains of 120%. Then, the strain to failure was discussed, based on an extension of the well-known Bridgman's model, to specimens drawn from sheet metal, exhibiting a rectangular cross-section. This thorough, but non exhaustive discussion of the material behavior, was followed by an analysis of strain localization during sheet forming. The main factors controlling strain localization and consequent damage were offered.

A new damage criterion by Bacha et al., particularly suited for small stress triaxiality and large material rotations was introduced. This predicts perfectly hemming behavior. Finally, the chapter finished with a novel analysis of hemming. Clearly, strain localization defines hemming limits. This hemming model (based on sheet geometry, grain size, and PSC measured large-strain behavior) is a powerful tool for alloy design.

Acknowledgements

Author details

Helmut Klöcker[1]* and Christopher Yukna[2]

*Address all correspondence to: klocker@emse.fr

1 Materials Science and Mechanical Engineering, École des Mines de Saint-Étienne, France

2 Department of Languages, École des Mines de Saint-Étienne, France

References

[1] Gurland J, Plateau J. The mechanism of ductile rupture of metals containing inclusions. Transactions of American Society for Metals. 1963;**56**:442-454

[2] McClintock FA. A criterion for ductile fracture by the growth of holes. Journal of Applied Mechanics. 1968;**35**:363-371

[3] Rice JB, Tracey DM. On the ductile enlargement of voids in triaxial stress fields. Journal of the Mechanics and Physics of Solids. 1969;**17**:201-217

[4] Koplik J, Needleman A. Void growth and coalescence in porous plastic solids. International Journal of Solids and Structures. 1988;**24**:835-853

[5] Gurson AL. Continuum theory of ductile rupture by void nucleation and growth: Part I – 10 Yield criteria and flow rules for porous ductile media. Journal of Engineering Materials and Technology. 1977;**99**:2-15

[6] Le Roy G, Embury JD, Edwards G, Ashby MF. Model of ductile fracture based on the nucleation and growth of voids. Acta Metallurgica. 1981;**29**:1509-1522

[7] Hutchinson JW, Tvergaard V. Shear band formation in plane strain. International Journal of Solids Structures. 1981;**17**:451-470

[8] Marciniak Z, Kuczynski K. Limit strains in the processes of stretch-forming sheet metal. International Journal of Mechanical Sciences. 1967;**9**:609-620

[9] Watts AB, Ford H. On the basic yield stress curve for a metal. Proceedings of the Institution of Mechanical Engineers. 1955;**169**(14):1141-1156

[10] Vegter H, ten Hor CHLJ, An Y, Atzema EH, Pijlman HH, van den Boogaard TH, Huetink H. Characterisation and modelling of the plastic material behaviour and its application in sheet metal forming simulation. In: Onate E, Owen DR, editors. VII International Conference on Computational Plasticity, Complas VII; Barcelona; 2003. pp. 1-20

[11] Maurice CI, Driver JH. High temperature plane strain compression of cube-oriented aluminium crystals. Acta Metallurgica et Materialia. 1993;**41**:1653-1664

[12] Maurice CI, Piot D, Klöcker H, Driver JH. Hot plane strain compression testing of aluminium alloys by channel-die compression. Metallurgical and Materials Transactions A. 2005;**36A**:1039-1047

[13] Bacha A, Maurice Cl, Klöcker H, Driver JH. The large strain flow stress behaviour of aluminium alloys as measured by channel-die compression (20-500°C). Materials Science Forum. 2006;**519-521**:783-788

[14] Orlans-Joliet B, Driver JH, Montheillet F. Plane strain compression of silicon-iron single crystals. Acta Metallurgica et Materialia. 1990;**38**:581-594

[15] Bacha A, Daniel D, Klöcker H. On the determination of true stress triaxiality in sheet metal. Journal of Materials Processing Technology. 2007;**184**:272-287

[16] Brunet M, Morestin F. Experimental and analytical necking studies of anisotropic sheet metals. Journal of Materials Processing Technology. 2001;**112**:214-226

[17] Driver JH, Skalli A. L'essai de compression plane de monocristaux encastrés: méthode d'étude du comportement d'un cristal soumis à une déformation plastique imposée. Revue de Physique Appliquee. 1983;**17**:447-451

[18] Voce E. The relationship between stress and strain for homogeneous deformation. Journal of Institute of Metals. 1948;**74**:537-562

[19] Voce E. True stress-strain curves and their application to cold-working processes. Metal Treatment. 1948;**15**:53-60

[20] Barlat F, Maeda Y, Chung K, Yangawa M, Brem JC, Hayashida Y, Lege DJ, Matsui K, Murtha SJ, Hattori S, Becker RC, Makosey S. Yield function development for aluminum alloy sheets. Journal of the Mechanics and Physics of Solids. 1997;**45**(11/12):1727-1763

[21] Klöcker H, Tvergaard V. Void growth and coalescence in metals deformed at elevated temperature. International Journal of Fracture. 2000;**106**:259-276

[22] Pardoen T, Hutchinson JW. An extended model for void growth and coalescence. Journal of the Mechanics and Physics of Solids. 1999;**48**(12):2467-2512

[23] Siebel E, Pomp A. Mitteilungen Kaiser-Wilhelm Inst. für Eisenforschung. Vol. 9; 1927. p. 157-165

[24] Leblond JB, Perrin G, Suquet P. Exact results and approximate models for porous viscoplastic solids. International Journal of Plasticity. 1994;**10**:213-235

[25] Tvergaard V. Influence of void nucleation on ductile shear fracture at a free surface. Journal of the Mechanics and Physics of Solids. 1984;**32**:373-393

[26] Bridgman W. The stress distribution at the neck of a tension specimen. Transactions of American Society for Metals. 1944;**32**:553-574

[27] Needleman A. A numerical study of necking in circular cylindrical bars. Journal of the Mechanics and Physics of Solids. 1972;**20**:111-127

[28] Tvergaard V. Necking in tensile bars with rectangular cross-section. Computer Methods in Applied Mechanics and Engineering. 1993;**103**:273-290

[29] Zhang ZL, Hauge M, Ødegård J, Thaulow C. Determining material true stress-strain curves from tensile specimens with rectangular cross-section. International Journal of Solids and Structures. 1999;**36**:3497-3516

[30] Bacha A, Daniel D, Klocker H, editors. Jürgen Hirsch, Birgit Skrotzki, Günter Gottstein, trimming of aluminium sheets: experimental and numerical investigations. ICAA11; 2008. pp. 1829-1835

[31] Benzarga AA, Besson J, Batisse R, Pineau A. Synergistic effects of plastic anisotropy and void coalescence on fracture mode in plane strain. Modelling and Simulation in Materials Science and Engineering. 2002;**10**:73-102

[32] Budiansky B, Hutchinson JW, Slutsky S. Void growth and collapse in viscous solids. In: Hopkins HG, Sewell MJ, editors. Mechanics of Solids, The R. Hill 60th Anniversary Volume; 1982. pp. 13-44

[33] Huang Y. Accurate dilatation rates for spherical voids in triaxial stress fields. Transactions of the ASME, Journal of Applied Mechanics. 1991;**58**:1084-1085

[34] Tvergaard V. On localisation in ductile materials containing spherical voids. International Journal of Fracture. 1982;**18**:237-252

[35] Tvergaard V, Needleman A. Analysis of the cup-cone fracture in a round tensile bar. Acta Metallurgica. 1984;**32**:157-169

[36] Bacha A, Feuerstein M, Desrayaud Ch, Klöcker H. Measuring stress strain curves to large strain on sheet metal. Journal of Testing and Evaluation. 2007;**35**(2):157-166

[37] Bao Y, Wierzbicki T. On fracture locus in the equivalent strain and stress triaxiality space. International Journal of Mechanical Sciences. 2004;**46**:81-98

[38] Bacha A, Daniel D, Klöcker H. Metal ductility at low stress triaxiality application to sheet trimming. Journal of Materials Processing Technology. 2008;**203**:480-497

[39] Bacha A, Daniel D, Klöcker H., ed. Jürgen Hirsch, Birgit Skrotzki, Günter Gottstein, Crack deviation during trimming of aluminium automotive sheets. ICAA11. 2008

[40] Bacha A, Daniel D, Klöcker H. Crack deviation during trimming of aluminium automotive sheets. Journal of Materials Processing Technology. 2010;**210**(14):1885-1897

[41] Thomason PF. Ductile Fracture of Metals. Oxford: Pergamon Press; 1990

[42] Gosh S, Li M, Khadke A. 3D modelling of shear slitting process for aluminium alloys. Journal of Material Processing Technology. 2005;**167**:91-102

[43] Atkins AG. On cropping and related processes. International Journal of Mechanical Sciences. 1980;**22**:215-225

[44] Zhou Q, Wierzbicki T. A tension zone model of blanking and tearing of ductile metal plates. International Journal of Mechanical Sciences. 1996;**38**:303-324

[45] Li M, Fata G. Sliver reduction in trimming aluminium autobody sheet. SAE Technical Paper Series, ed. European Aluminium Association; 1999-01-0661; 1999

[46] Li M. Method and apparatus for trimming aluminium sheet, United States Patent Application Publication, US2002/0017173A1; 2000

[47] Li M. An experimental investigation on cut surface and burr in trimming aluminium autobody sheet. International Journal of Mechanical Sciences. 2002;**42**:889-906

[48] Lloyd DJ, Gupta AK. In: Chandra T, Sakai T, editors. On the precipitation-hardening behavior of the Al-Mg-Si-Cu alloy AA6111. THERMEC'97, TMS; 1997. pp. 99-107

[49] Miller WS, Zhuang I, Bottema J, Wittebrood AJ, De Smet P, Haszler A, Vieregge A. Recent development in aluminium alloys for the automotive industry. Materials Science and Engineering: A. 2000;**A280**:37-49

[50] Minoda T, Asano M, Yoshida H. Influence of iron content on the mechanical properties of AA6016 alloy sheet, Materials Science Forum. 2006;**519-521**:859-864

[51] Sarkar J, Kutty TRG, Wilkinson DS, Embury JD, Lloyd DJ. Tensile properties and bendability of T4 treated AA6111 aluminium alloys. Materials Science and Engineering: A. 2004;**A369**:258-266

[52] Kuroda M, Tvergaard V. A phenomenological plasticity model with non-normality effects representing observations in crystal plasticity. Journal of the Mechanics and Physics of Solids. 2001;**49**:1239-1263

[53] Triantafyllidis N, Needleman A. On the development of shear bands in pure bending. International Journal of Solids and Structures. 1982;**18**(2):121-138

[54] Kuroda M, Tvergaard V. Effects of texture on shear band formation in plane strain tension/compression and bending. International Journal of Plasticity. 2007;**23**(2):244-272

[55] Becker R. Effects of strain localization on surface roughening during sheet forming. Acta Metallurgica. 1998;**46**(4):1385-1401

[56] Dao M, Li M. A micromechanics study on strain localization induced fracture initiation in bending using crystal plasticity models. Philosophical Magazine A. 2001;**81**(8):1997-2020

[57] Borland JC. Fundamentals of solidification cracking in welds.-II. Welding and Metal Fabrication. 1979;**33**:505-508

[58] Selcuk A, Rawlings RD. A Cantilever-type bend test technique for formability analysis of strip/plate metals. Journal of Testing and Evaluation. 1991;**19**:349-358

[59] Mattei L, Daniel D, Guiglionda G, Klöcker H. Hemming of aluminium automotive sheet. In: Hirsch J, Skrotzki B, Gottstein G, editors. ICAA 11, Aluminium Alloys, Their Physical and Mechanical Properties; 2008. pp. 1829-1835

[60] Mattei L, Daniel D, Guiglionda G, Klöcker H, Driver JH. Strain localization and damage mechanisms during bending of AA6016 sheet. Materials Science and Engineering: Sheet. Materials Science and Engineering A. 2012;**559**:812-821

[61] Mattei L, Daniel D, Guiglionda G, Moulin N, Klöcker H, Driver JH. Grain scale modelling of the bendability of AA6xxx Al alloy sheet. Materials Science and Engineering: A. 2013;**583**:96-104